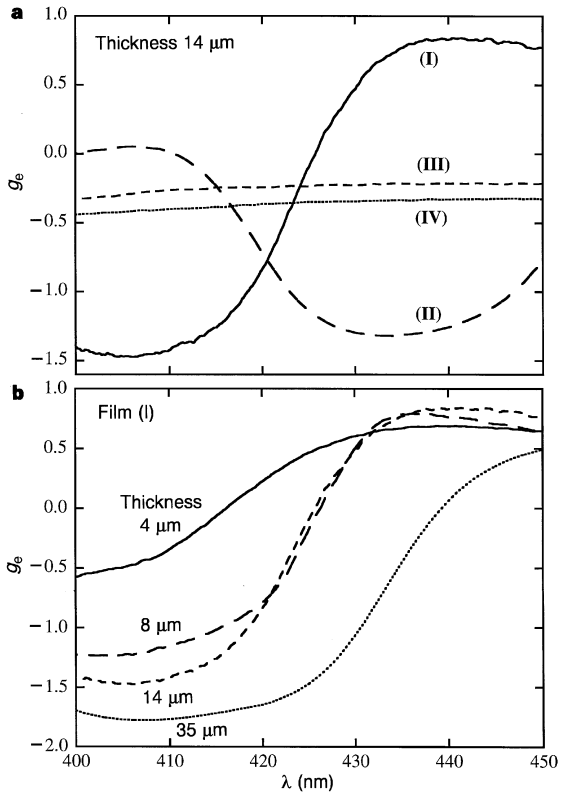

Figure 3 Dissymmetry factor (g_e) calculated from the CPPL spectra. **a**, Films (I), (II), (III) and (IV), all 14 μm thick; **b**, effect of film thickness on g_e displayed for (I). The reported g_e curves are reproducible to within ±5% in general.

As shown in Fig. 3a, films (III) and (IV) produced a small, negative g_e that remains largely constant throughout the spectral region, supporting the assumption that the emission of Exalite 428 is characterized by a single dipole moment parallel to the long molecular axis. In sharp contrast to the typical CPPL behaviour outside the resonance region, films (I) and (II) show emission in the resonance region, resulting in a large g_e that undergoes handedness reversal in a single-handed chiral-nematic host. This is an observation inexplicable by CPPL theory, in contrast to emission outside the resonance region[13,15]. The effect of thickness on g_e for film (I) is assessed in Fig. 3b, revealing the general cross-over behaviour for all thicknesses. We found nearly pure right-handed photoluminescence, manifested as g_e approaching −2, in the 400–420 nm wavelength range at a thickness of 35 μm. In addition, the single-photon counting technique was employed to determine the excited-state lifetime, t_{ex}. For emission outside the resonance region, a constant $t_{ex} = 0.66 \pm 0.02$ ns across the emission spectrum was found. For emission inside the resonance region, we found $t_{ex} = 0.67 \pm 0.02$ ns. The lack of a prolonged t_{ex} inside the resonance region alone seems to suggest the absence of microcavity processes.

Well aligned solid films with superior morphological stability hold promise for practical applications. Specific examples include colour image projection[10] and stereoscopic displays[11] that have been proposed on the basis of non-emitting chiral-nematic films. Furthermore, embedding laser dyes in vitrified chiral-nematic films has the potential to realize low-threshold distributed feedback lasers[17], with a cost advantage over inorganic semiconductor lasers. □

Received 11 June; accepted 30 November 1998.

1. Dirix, Y., Tervoort, T. A. & Bastiaansen, C. Optical properties of oriented polymer/dye polarizers. *Macromolecules* **28,** 486–491 (1995).
2. Schadt, M. & Fünfschilling, J. New liquid crystal polarized color projection pinciple. *Jpn J. Appl. Phys.* **29,** 1974–1984 (1990).
3. Montali, A., Bastiaansen, C., Smith, P. & Weder, C. Polarizing energy transfer in photoluminescent materials for display applications. *Nature* **392,** 261–264 (1998).
4. Dyreklev, P. *et al.* Polarized electroluminescence from an oriented substituted polythiophene in a light emitting diode. *Adv. Mater.* **7,** 43–45 (1995).
5. Era, M., Tsutsui, T. & Saito, S. Polarized electroluminescence from oriented *p*-sexiphenyl vacuum-deposited film. *Appl. Phys. Lett.* **67,** 2436–2438 (1995).
6. Cimrová, V., Remmers, M., Neher, D. & Wegner, G. Polarized light emission from LEDs prepared by the Langmuir-Blodgett technique. *Adv. Mater.* **8,** 146–149 (1996).
7. Sariciftci, N. S., Lemmer, U., Vacar, D., Heeger, A. J. & Janssen, R. A J. Polarized photoluminescence of oligothiophenes in nematic liquid crystalline matrices. *Adv. Mater.* **8,** 651–654 (1996).
8. Lüssem, G. *et al.* Polarized electroluminescence of light emitting liquid crystalline polymers. *Liq. Cryst.* **21,** 903–907 (1996).
9. Chen, S. H., Shi, H., Conger, B. M., Mastrangelo, J. C. & Tsutsui, T. Novel vitrifiable liquid crystals as optical materials. *Adv. Mater.* **8,** 998–1001 (1996).
10. Heynderickx, I. E. J. R. & Broer, D. J. Illumination system for a color projection device and circular polarizer suitable for use in such an illumination system, and color image projection device comprising such an illumination system and circular polarizer. US Patent No. 5,626,408 (1997).
11. Hall, D. R. Use of stereoscopic systems utilizing chiral liquid crystals. US Patent No. 5,699,184 (1997).
12. Langeveld-Voss, B. M. W. *et al.* Circular dichroism and circular polarization of photoluminescence of highly ordered poly{3,4-di[(*S*)-2-methylbutoxy]-thiophene}. *J. Am. Chem. Soc.* **118,** 4908–4909 (1996).
13. Shi, H., Conger, B. M., Katsis, D. & Chen, S. H. Circularly polarized fluorescence from chiral nematic liquid crystalline films: theory and experiment. *Liq. Cryst.* **24,** 163–172 (1998).
14. Peeters, E. *et al.* Circularly polarized electroluminescence from a polymer light-emitting diode. *J. Am. Chem. Soc.* **119,** 9909–9910 (1997).
15. Katsis, D., Schmid, A. W. & Chen, S. H. Mechanistic insight into circularly polarized photoluminescence from a chrial-nematic film. *Liq. Cryst.* (in the press).
16. Wu, S. T., Efron, U. & Hess, L. D. Birefringence measurements of liquid crystals. *Appl. Opt.* **23,** 3911–3915 (1984).
17. Il'chishin, I. P., Tikhonov, E. A., Tishchenko, V. G. & Shpak, M. T. Generation of a tunable radiation by impurity cholesteric liquid crystals. *JETP Lett.* **32,** 24–27 (1981).

Acknowledgements. We thank R. W. Boyd, L. J. Rothberg and S. D. Jacobs for discussions. This work was supported by the US National Science Foundation, US Department of Energy, and the Japanese Ministry of International Trade and Industry.

Correspondence and requests for materials should be addressed to S.H.C. at the University of Rochester (e-mail: shch@lle.rochester.edu).

Accelerated dissolution of diatom silica by marine bacterial assemblages

Kay D. Bidle & Farooq Azam

Marine Biology Research Division, 0202, Scripps Institution of Oceanography, University of California San Diego, La Jolla, California 92093, USA

Downward fluxes of biogenic silica and organic matter in the global ocean derive dominantly from the productivity of diatoms—phytoplankton with cell walls containing silica encased in an organic matrix[1,2]. As diatoms have an absolute requirement for silicon (as silicic acid)[3], its supply into the photic zone—largely by silica dissolution and upwelling—controls diatom production (and consequently the biological uptake of atmospheric CO_2 by the ocean) over vast oceanic areas[4]. Current biogeochemical models assume silica dissolution to be controlled by temperature, zooplankton grazing and diatom aggregation[4,5], but the role of bacteria has not been established. Yet bacteria utilize about half of the organic matter derived from oceanic primary production[6] by varied strategies, including attack on dead and living diatoms by using hydrolytic enzymes[7,8], and could adventitiously hasten silica dissolution by degrading the organic matrix which protects diatom frustules from dissolution[9,10]. Here we report the results of experiments in which natural assemblages of marine bacteria dramatically increased silica dissolution from two species of lysed marine diatoms compared to bacteria-free controls. Silica dissolution accompanied, and was caused by, bacterial colonization and hydrolytic attack. Bacteria-mediated silicon regeneration rates varied with diatom type and bacterial assemblage; observed rates could explain most of the reported upper-ocean silicon regeneration[5,11]. Bacteria-mediated silicon regeneration may thus critically control diatom productivity and the cycling and fate of silicon and carbon in the ocean.

In the recent concept of the "silicate pump"[4], diatom productivity

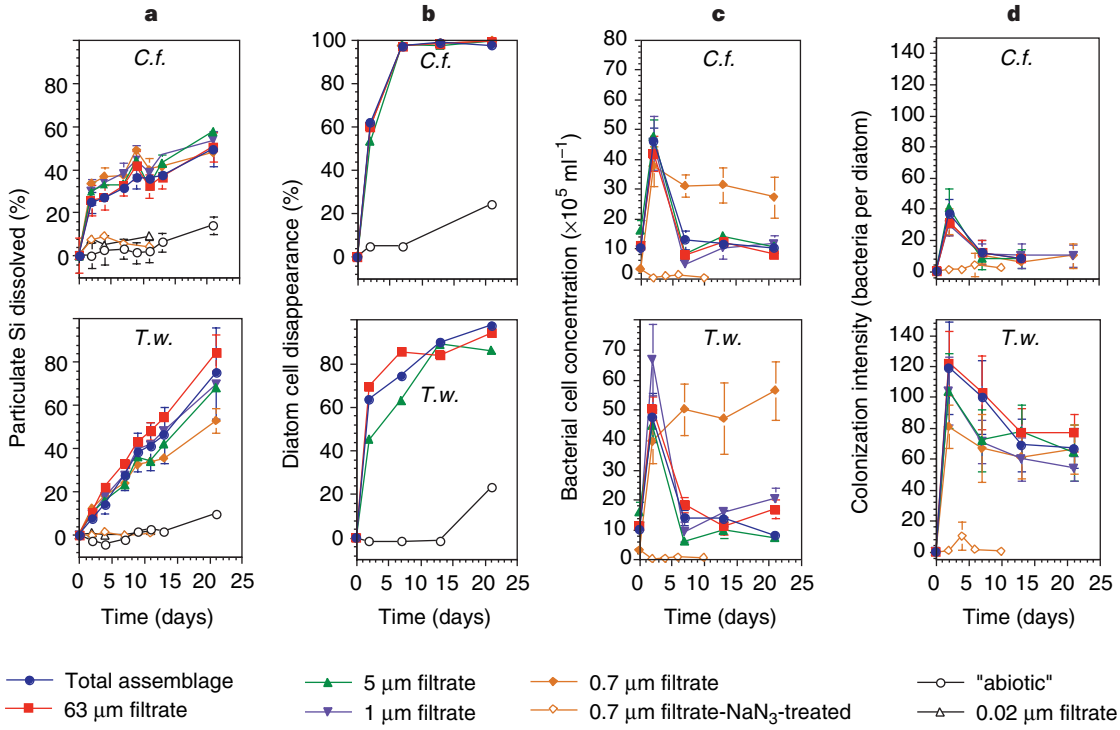

Figure 1 Bacterial colonization and silicon regeneration of diatoms lysed by freeze-thaw. (*C.f.*, *Cylindrotheca fusiformis*; *T.w.*, *Thalassiosira weissflogii*.) Diatom detritus was exposed to whole sea water, sea water filtered through various size filters, or 0.2-μm-filtered, autoclaved sea water ("abiotic") (see symbol key); additional samples were treated with sodium azide (50 mM) or suspended in 0.02-μm-filtered sea water. **a**, Dissolution of particulate silica; **b**, "disappearance" of diatoms (no longer visible in the epifluorescence microscope by their chlorophyll autofluorescence or other cell components); **c**, bulk-phase bacterial concentrations; and **d**, bacterial colonization intensity.

in open-ocean upwelling systems becomes silicon-limited because of selective recycling of nitrogen over silicon: zooplankton grazing on diatoms efficiently regenerates nitrogen within the upper mixed layer but packages silica in faecal pellets, transporting it to depth where it dissolves to silicic acid. Consequently, silicic acid supply rate (rather than iron or nitrate) by upwelling sets the upper limit on diatom productivity and export production. On the other hand, substantial and highly variable silicon regeneration has been observed within the water column in several oceanic systems[5,11]. The global-mean biogenic silica dissolution: production (D:P) ratio is 0.58 (0.05–5.8; ref. 5) with silicon regeneration supporting much (>70%) of the biogenic silica production (diatom growth) in a coastal upwelling area[12], within a warm core ring[13] and in the Ross Sea continental shelf waters[1]. These contradictory views of silicon regeneration raise questions about its mechanism and regulation in the upper mixed layer. Silica dissolution from diatom frustules has been considered as being mainly due to chemical depolymerization[10] not involving biological activity, as metazoan grazing did not enhance regeneration[14,15]. However, the role of bacteria and the microbial loop in silicon regeneration has not been explicitly examined. Significant silicon regeneration by bacteria would cause a 'leak' in the silica pump, accounting for the high and variable D:P ratios. Pelagic marine bacteria colonize fresh diatom detritus[16], living diatoms[8] and "marine snow" phytoaggregates[7] with colonizers expressing very high levels of hydrolytic ectoenzymes (protease, α- and β-glucosidase, alkaline phosphatase, lipase and chitinase). Bacterial hydrolytic attack on diatom cell walls would denude silica of its organic coating and hasten its dissolution.

We tested whether the action of natural, pelagic marine bacterial assemblages on lysing diatoms could accelerate silica dissolution. Our focus was on lysed diatoms because a substantial fraction of diatom productivity, especially after blooms, can escape grazing[17] and instead undergoes cell lysis in response to physiological stress[18,19]. We used freeze-thaw-lysed axenic cultures of diatom cells; they provided the well-characterized diatom detritus of known history necessary for addressing the mechanistic relationships between bacterial action on diatom detritus and silicon regeneration. Two diatoms were studied, one lightly silicified (*Cylindrotheca fusiformis*; ~60 fmol Si per cell) and one heavily silicified (*Thalassiosira weissflogii*; ~800 fmol Si per cell). We were mainly interested in regeneration kinetics during the first ~10 d, a conservative estimate of the residence time of unaggregated diatom detritus in the upper mixed layer. Lysed diatoms were suspended in whole sea water or in sea water which had been filtered through various pore sizes: 0.2-μm-filtered-autoclaved ("abiotic"), 0.02-μm Whatman Anodisc, GF/F 0.7 μm ("bacterial fraction"), 1-μm Nuclepore, and 5-μm and 63-μm Nitex. This was done to test the contribution of bacterial action to silicon regeneration relative to other trophic levels (for example, protozoa). The added diatom detritus ($(1–3) \times 10^4$ ml^{-1}) and the resulting silica concentrations ($(2–6)$ μg Si l^{-1}) were comparable to those during a moderate bloom. We followed silica dissolution and its relationship to microbial populations, particularly those colonizing the detritus, during incubations which were conducted at near-ambient temperature (16–18 °C). Seawater pH (7.9–8.1) did not change during incubation.

When suspended in "abiotic" sea water, the silica of both diatoms was remarkably resistant to dissolution (*C. fusiformis*, $0.2 \pm 0.3\%$ d^{-1}; *T. weissflogii*, $0.3 \pm 0.2\%$ d^{-1}; Fig. 1a). Similarly, low rates (*C. fusiformis*, $0.9 \pm 0.3\%$ d^{-1}; *T. weissflogii*, $0.2 \pm 0.1\%$ d^{-1}; Fig. 1a) were found for diatoms incubated in filtered (0.02-μm pore size), unautoclaved sea water, thus arguing against the involvement of any *in situ* dissolved hydrolases present in sea water or released during filtration. Dissolution was dramatically faster in 0.7-μm-filtered sea water (Fig. 1a), with initial rates

Table 1 Particulate silica dissolution and turnover rates

Diatom	Experiment	Particulate silica dissolved (%)*	Turnover rate (% d^{-1})†	
			Day 0–2	Day >2‡
C. fusiformis	1	81 ± 6.9	4.6 ± 2.8	2.2 ± 0.8
	2	70 ± 1.5	8.2 ± 0.5§	1.5 ± 1.5§
	3‖	48 ± 2.7	18 ± 1.7	0.8 ± 4.1
	4‖	52 ± 3.2	17 ± 1.2	0.8 ± 3.2
T. weissflogii	1	53 ± 4.5	2.1 ± 1.2	2.0 ± 0.9
	2	71 ± 0.9	4.0 ± 0.1	2.3 ± 0.8§
	3‖	55 ± 5.7	6.1 ± 0.7	2.7 ± 1.2
	4‖	62 ± 4.0	7.9 ± 0.6	3.2 ± 0.2

Data shown are for diatom detritus exposed to natural bacterial assemblages (<0.7 μm).
* At end of experiment (21–31 days); values are shown ± s.d.
† Values are shown ± s.d.
‡ Average turnover rate.
‖ Water for experiments 3 and 4 was collected at the same time.
§ Day 0–3.

of 18 ± 1.7% d^{-1} for *C. fusiformis* and 7.9 ± 0.7% d^{-1} for *T. weissflogii*. Regeneration rates were not significantly different when diatom detritus was suspended in the larger size fractions of sea water or in whole sea water (Fig. 1a). Time courses of silica regeneration for the two diatoms were distinctly different, perhaps reflecting differences in the degree of cell-wall silicification as well as cell-wall architecture and chemistry. Turnover rates for the highly silicified *T. weissflogii* were initially lower but later exceeded the *C. fusiformis* rates (Table 1). Consistent with rapid silica dissolution, epifluorescence microscopy showed that lysed diatoms 'disappeared' (sometimes visible as 'ghosts') roughly in parallel with, or faster than, silica dissolution (Fig. 1b). Using epifluorescence and dark-field microscopy, no protozoa were detected in the <0.7-μm fraction nor were any bacteria detected in the <0.02-μm or "abiotic" fractions (except in the 21-d sample for the latter; and this was accompanied by increased silica dissolution). Thus, the <0.02-μm and <0.2-μm incubations were indeed abiotic and the only known biological activity acting on diatom detritus in <0.7-μm incubations would be due to Bacteria (and possibly Archaea[20]).

In addition to the size-fractionation data, mentioned above, the following lines of evidence suggest that silicon regeneration was indeed caused by bacteria and that the mechanism involved detritus colonization and hydrolytic attack on organic matrix. Sodium azide (50 mM) either strongly inhibited silicon regeneration or abolished it completely (Fig. 1a), roughly in parallel with inhibition of bacterial colonization of detritus (Fig. 1d) and activity. A mixture of penicillin, streptomycin and chloramphenicol, which should have inhibited the activities of many prokaryotes (it inhibited but did not abolish prokaryotic growth in <0.7-μm incubations) also inhibited silica dissolution by 50% after 7–11 d for *C. fusiformis* but no effect was observed for *T. weissflogii*. All biotic incubations showed strong and rapid colonization of diatom detritus by bacteria (bacterial concentration was 10^{11} ml^{-1} in the detritus microenvironment, 10^5 times the bulk-phase concentration; Table 2). Colonization intensity, rather than bulk-phase bacterial abundance, appeared to control silicon regeneration. Colonization intensity and silicon regeneration rates were similar among all biotic incubations, even when bulk-phase bacteria concentrations were very different (for example, <0.7-μm incubations; Fig. 1c); thus, variation in bulk-phase bacterial concentrations and activity may not control silica regeneration. Further, the distinctly different patterns of persistence of colonization for *C. fusiformis* and *T. weissflogii* (Fig. 1d) corresponded to distinctly different time courses of silicon regeneration (Fig. 1a). The colonizing bacteria had high growth rates and imparted extremely high protease activities to the diatom detritus microenvironment (Table 2). Glycoproteins are significant components of diatom cell walls and are thought to be involved in frustule biogenesis[21] so their hydrolysis by proteases may have hastened silica solubilization. To test that protease action was important in organic matrix dissolution and silica dissolution we incubated uniformly ^{14}C-labelled diatom detritus with pronase E (0.1 unit ml^{-1}) in the absence of bacteria. Pronase E rapidly released ^{14}C as well as regenerated silicon at moderate rates (Fig. 2). The pattern of silica dissolution for each diatom following pronase E treatment was similar to that in bacterial treatments (Fig. 1a). Pronase E digestion also yielded distinctly different patterns for the two diatoms in the regeneration of particulate carbon and silicon, presumably reflecting differences in cell-wall structure and perhaps chemical composition.

Rates of bacteria-mediated silica dissolution (Table 1; day 0–2;) were as fast as those reported for acid-digested frustules at a slightly higher temperature (5.5–18% d^{-1}; ref. 9), suggesting that bacteria can efficiently remove the organic matrix. If we assume an average sinking rate of 1 m d^{-1} (ref. 22) and a 20-m mixed-layer depth, then bacteria-mediated dissolution would regenerate 49–51% and 40–73% of silicon from *C. fusiformis* and *T. weissflogii* detritus, respectively (Table 1). These values are comparable to the vertically integrated global-average silica D:P ratio of 0.58 (ref. 5) consistent with an important role for bacteria in silicon regeneration in the sea. Clearly, the *in situ* regeneration rates will be modulated by other ecosystem parameters, particularly those affecting bacterial activity on diatoms. Temperature is commonly considered the main control on diatom silica dissolution[23]. Our finding of bacterial mediation of dissolution suggests that temperature controls not only the chemical depolymerization of silica[10] but also the action of bacteria on the organic matrix. Its effect on these two processes is probably sequential and differential, and needs to be elucidated to understand the behaviour of diatom frustules experiencing changing temperature (for example, during sinking). Temperature effects on bacterial metabolism may account for diatom frustules having dissolution coefficients in sea water with a temperature coefficient, Q_{10}, of 2.27 (ref. 9; the study used diatoms collected in net-tows and incubated in 0.45-μm-filtered sea water and probably contained active bacteria). Bacterial species composition and/or metabolic

Table 2 Bacterial colonization and activity on diatom cell detritus

Diatom	Time (d)	Colonization intensity (bacteria $cell^{-1}$)	Attached bacteria l^{-1} ($\times 10^{12}$)	Bacteria concentration ratio (Att/FL)*	Cell-specific protease hydrolysis activity (amol $cell^{-1}$ h^{-1})	Protease activity ratio† (Att./FL)	Cell-specific growth rate (d^{-1})
C. fusiformis	0	–	–	–	17 ± 1.8‡	–	0.04 ± 0.01‡
	1	12 ± 6	40	28,500	84 ± 65	12,900	1.78 ± 1.42
	2	56 ± 14	190	17,500	2,505 ± 1,680	39,100	0.85 ± 1.52
	4	38 ± 16	120	7,200	647 ± 566	6,400	1.66 ± 3.85
T. weissflogii	0	–	–	–	29 ± 4.7‡	–	0.05 ± 0.01‡
	1	16 ± 12	40	27,900	324 ± 274	26,500	2.27 ± 1.92
	2	108 ± 38	270	23,200	4,058 ± 2,698	78,500	1.33 ± 0.95
	4	98 ± 30	250	9,200	11,217 ± 18,781	155,000	6.65 ± 11.5

See Methods for details of experimental procedure.
* Att., attached bacteria; FL, free-living bacteria.
† Activities were calculated per unit voume (ml); see Methods.
‡ Day 0 values are for bulk sea water.

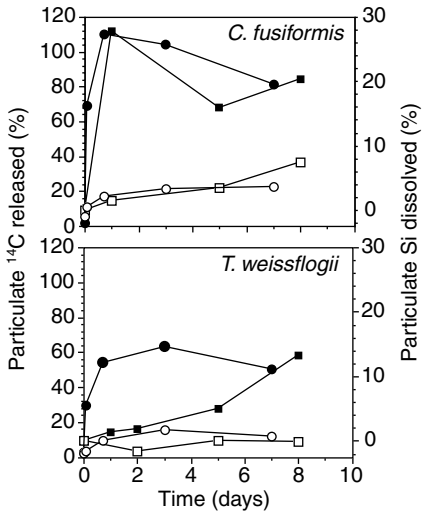

Figure 2 Pronase E digestion of *C. fusiformis* or *T. weissflogii* detritus. Left-hand vertical axis, release of particulate ^{14}C due to pronase E addition to uniformly ^{14}C-labelled detritus (open circles, control; filled circles, pronase E addition). Right-hand vertical axis, dissolution of particulate silica caused by pronase E to unlabelled detritus (open squares, control; filled squares, pronase E addition). Control incubations consisted of diatom detritus suspended in 0.2-μm-filtered, autoclaved sea water (no pronase E added).

state appear to be important variables in bacteria-mediated silicon regeneration, as assemblages collected on different days yielded ~4-fold variation in initial regeneration rate (Table 1). Diatom aggregation into marine snow may also enhance silica solubilization[24], probably because aggregates harbour high bacterial concentrations expressing intense ectohydrolase activities[7]. Finally, trophic interactions, such as protozoan grazers and viruses controlling bacteria abundance and activity, may regulate silicon regeneration. Thus, bacteria mediate potentially rapid but highly variable silicon regeneration rates which are regulated not only by temperature but also by multifaceted *in situ* controls on bacterial action on diatom frustules.

Bacteria-mediated silicon regeneration rates from our model system can not *a priori* be extrapolated to the ocean, yet our results provide mechanistic insights on control of diatom productivity as well as illustrating the potential for a greater importance of diatoms in oceanic carbon biogeochemistry. High and variable D:P ratios (0.5–0.8) for open-ocean systems[5,11] can now be interpreted as being caused mainly by bacteria (because we found little abiotic or protozoa-mediated dissolution, and because metazoa did not cause dissolution[15]. Protozoa grazing on nanoplanktonic diatoms may contribute but this is unstudied). Our estimates of silicon regeneration (40–73%) together with field D:P ratios indicate that bacteria-mediated silicon regeneration is of quantitative significance for oceanic diatom biogeochemistry. It has implications for food-web structure and carbon cycling, particularly in open-ocean upwelling high-nutrient low-chlorophyll (HNLC) systems like the equatorial upwelling zone. Upwelled silicic acid is predicted to set the upper limit on diatom production by a model which assumes no silicon regeneration ("silicate pump"[4]). A D:P ratio of 0.5–0.8 (that is, 50–80% diatom production based on regenerated silicon) would reduce the diatom *f*-ratio (new production/total production) from 1.0 (predicted by the model) to 0.2–0.5 and would increase the predicted upper limit on diatom carbon fixation by 2–5 times through regenerated production. Depending on the relative supply rates of other nutrients (NO_3^- and Fe), diatom production may instead become N- or Fe-limited. In Monterey Bay and in coastal upwelling systems off Peru, even modest silicon regeneration (for example, a D:P ratio of 0.1) can shift diatom production from Si to N limitation[25]; similar reasoning might apply to HNLC waters which may oscillate between Si and Fe limitation. Thus the microbial loop may exert critical controls on diatom production and its biogeochemical fate in these oceanic systems. □

Methods

Silica dissolution measurements. Natural seawater samples taken from Scripps Pier were filtered through Nitex mesh (Tetko; 63- or 5-μm pore sizes), polycarbonate membrane filters (Poretics; 1.0- or 0.2-μm pore size), or Whatman filters (GF/F, 0.7-μm pore size and Anodisc, 0.02-μm pore size). Filtered (0.2-μm) autoclaved sea water was also prepared, and served as the control medium. Incubations were done in 300-ml Nalgene bottles. The spectrophotometric silicomolybdate assay described by Parsons *et al.*[26] was used to measure the concentration of dissolved silicic acid in incubated samples. Aliquots were sampled and particulate material was pelleted (3,000*g*; 15 min; 10 °C). The supernatant was assayed for silicic acid concentration. Total silica budgets in samples were determined by a hot sodium hydroxide hydrolysis technique[27]. All incubations and assays were done in sterile polypropylene containers.

Microscopy. Concentrations of diatoms and bacteria were determined by epifluorescence microscopy (Olympus BH-2). For diatoms, samples were filtered onto 0.8-μm, black Nuclepore filters and counted using autofluorescence (312× magnification). For bacteria, samples were filtered onto 0.2-μm, black Poretics filters after staining with 4,6-diamidino-2-phenyl indole 1 μg ml^{-1}; 10 min) and counted at 1,250× magnification. Average colonization intensities were obtained by counting the number of attached bacteria on at least 30 individual diatom cells. Attached bacterial concentrations in diatom detritus microenvironment were calculated by dividing average bacteria per diatom by diatom cell volume.

Bacterial production and ectoprotease measurements. Diatom detritus was exposed to 0.7-μm-filtered sea water. Protease activity and bacterial production were measured periodically in the total suspension and <3.0-μm-filtered samples. Cell-specific rates for attached bacteria were obtained on the basis of the difference between total and <3.0-μm fractions. Protease activities were measured using the fluorogenic substrate L-leucine-7-amino-4-methylcoumarin (ref. 28) added at a final concentration of 100 μM; samples were incubated at the *in situ* temperature (18 °C) in the dark. Assays were done in duplicate and one sample was boiled before addition of substrate and served as a control. Fluorescence was measured using a Hoefer TKO-100 fluorometer and was calibrated with 7-amino-4-methylcoumarin. Attached:free-living bacteria protease concentration ratios were calculated as the ratio of enzyme activity in equal volumes of diatom detritus and the bulk phase. Bacterial growth rates were determined by ^{3}H-leucine incorporation[29] during incubations at the *in situ* temperature (18 °C) in the dark. Cell-specific growth rate calculations assumed 20 fg C per cell (ref. 30). Assays were done in triplicate.

Pronase E treatment experiment. Release of carbon was measured for diatom detritus made from metabolically uniformly ^{14}C-labelled diatoms suspended in abiotic (0.2-μm-autoclaved) sea water. Parallel incubations with unlabelled diatom detritus were used to measure silicon regeneration. Pronase E (Sigma) was added to a final concentration of 0.1 unit ml^{-1}. Control samples were incubated in abiotic sea water only. Aliquots were removed periodically, centrifuged to sediment the detritus, and ^{14}C activity (labelled incubations) or silicic acid concentrations[26] (unlabelled incubations) were measured in the supernatant.

Received 18 June; accepted 23 October 1998.

1. Nelson, D. M., DeMaster, D. J., Dunbar, R. B. & Smith, W. O. Jr Cycling of organic carbon and biogenic silica in the Southern Ocean: estimates of water-column and sedimentary fluxes on the Ross Sea continental shelf. *J. Geophys. Res.* **101,** 18519–18532 (1996).
2. Longhurst, A. R. & Harrison, W. G. The biological pump: profiles of plankton production and consumption in the upper ocean. *Prog. Oceanogr.* **22,** 47–123 (1989).
3. Lewin, J. C. in *Physiology and Biochemistry of Algae* (ed. Lewin, R. E.) 445–455 (Academic, New York, 1962).
4. Dugdale, R. C. & Wilkerson, F. P. Silicate regulation of new production in the equatorial Pacific upwelling. *Nature* **391,** 270–273 (1998).
5. Nelson, D. M., Tréguer, P., Brzezinski, M. A., Leynaert, A. & Quéguiner, B. Production and dissolution of biogenic silica in the ocean: revised global estimates, comparison with regional data and relationship to biogenic sedimentation. *Glob. Biogeochem. Cycles* **9,** 359–372 (1995).
6. Cole, J. J., Findlay, S. & Pace, M. L. Bacterioplankton production in fresh and saltwater ecosystems: a cross-system overview. *Mar. Ecol. Prog. Ser.* **43,** 1–10 (1988).
7. Smith, D. C., Simon, M., Alldredge, A. L. & Azam, F. Intense hydrolytic enzyme activity on marine aggregates and implications for rapid particle dissolution. *Nature* **359,** 139–142 (1992).

8. Smith, D. C., Steward, G. F., Long, R. A. & Azam, F. Bacterial utilization of carbon fluxes during a diatom bloom in a mesocosm. *Deep-Sea Res. II* **42,** 75–97 (1995).
9. Kamatani, A. Dissolution rates of silica from diatoms decomposing at various temperatures. *Mar. Biol.* **68,** 91–98 (1982).
10. Lewin, J. C. The dissolution of silica from diatom walls. *Geochim. Geophys. Acta* **21,** 182–198 (1961).
11. Brzezinski, M. A. & Nelson, D. M. The annual silica cycle in the Sargasso Sea near Bermuda. *Deep-Sea Res. I* **42,** 1215–1237 (1995).
12. Nelson, D. M. & Goering, J. J. Near-surface silica dissolution in the upwelling region off northwest Africa. *Deep-Sea Res.* **24,** 65–73 (1977).
13. Brzezinski, M. A. & Nelson, D. M. Seasonal changes in the silicon cycle within a Gulf Stream warm-core ring. *Deep-Sea Res.* **36,** 1009–1030 (1989).
14. Cowie, G. L. & Hedges, J. I. Digestion and alteration of the biochemical constituents of a diatom (*Thalassiosira weissflogii*) ingested by a herbivorous zooplankton (*Calanus pacificus*). *Limnol. Oceanogr.* **41,** 581–594 (1996).
15. Tande, K. S. & Slagstad, D. Assimilation efficiency in herbivorous aquatic organisms—the potential of the ratio method using ^{14}C and biogenic silica as markers. *Limnol. Oceanogr.* **30,** 1093–1099 (1985).
16. Biddanda, B. A. & Pomeroy, L. R. Microbial aggregation and degradation of phytoplankton-derived detritus in seawater. I. Microbial succession. *Mar. Ecol. Prog. Ser.* **42,** 79–88 (1988).
17. Brussaard, C. P. D. *et al*. Effects of grazing, sedimentation and phytoplankton cell lysis on the structure of a coastal pelagic food web. *Mar. Ecol. Prog. Ser.* **123,** 259–271 (1995).
18. Berges, J. A. & Falkowski, P. G. Physiological stress and cell death in marine phytoplankton: induction of proteases in response to nitrogen or light limitation. *Limnol. Oceanogr.* **43,** 129–135 (1998).
19. Brussaard, C. P. D., Noordeloos, A. A. M. & Riegman, R. Autolysis kinetics of the marine diatom *Ditylum brightwellii* (Bacillariophyceae) under nitrogen and phosphorus limitation and starvation. *J. Phycol.* **33,** 980–987 (1997).
20. DeLong, E. Archael means and extremes. *Science* **280,** 542–543 (1998).
21. Kröger, N., Bergsdorf, C. & Sumper, M. A new calcium binding glycoprotein family constitutes a major diatom cell wall component. *EMBO J.* **13,** 4676–4683 (1994).
22. Smayda, T. J. The suspension and sinking of phytoplankton in the sea. *Oceanogr. Mar. Biol. Annu. Rev.* **8,** 353–414 (1970).
23. Kamatani, A. & Riley, J. P. Rate of dissolution of diatom silica walls in seawater. *Mar. Biol.* **55,** 29–35 (1979).
24. Brzezinski, M. A., Alldredge, A. L. & O'Bryan, L. M. Silica cycling within marine snow. *Limnol. Oceanogr.* **42,** 1706–1713 (1997).
25. Brzezinski, M. A., Phillips, D. R., Chavez, F. P., Friederich, G. E. & Dugdale, R. C. Silica production in the Monterey, California, upwelling system. *Limnol. Oceanogr.* **42,** 1694–1705 (1997).
26. Parsons, T. R., Maita, Y. & Lalli, C. M. *A Manual of Chemical and Biological Methods for Seawater Analysis* (Pergamon, Oxford, 1984).
27. Werner, D. Die Kieselsäure im Stoffwechsel von *Cyclotella cryptica* Reimann, Lewin und Guillard. *Arch. Mikrobiol.* **55,** 278–308 (1966).
28. Hoppe, H. G. Significance of exoenzymatic activities in the ecology of brackish water: measurements by means of methylumbelliferyl-substrates. *Mar. Ecol. Prog. Ser.* **11,** 299–308 (1983).
29. Smith, D. C. & Azam, F. A simple, economical method for measuring bacterial protein synthesis rates in seawater using ^{3}H-leucine. *Mar. Microb. Food Webs* **6,** 107–114 (1992).
30. Lee, S. & Fuhrman, J. A. Relationships between biovolume and biomass of naturally derived marine bacterioplankton. *Appl. Environ. Microbiol.* **53,** 1298–1303 (1987).

Acknowledgements. We thank D. C. Smith, M. Hildebrand, M. A. Brzezinski, J. T. Hollibaugh and K. A. Bidle for discussions and suggestions. This work was supported by NSF grants to F.A.

Correspondence and requests for materials should be addressed to F.A. (e-mail: fazam@ucsd.edu).

Cool surface waters of the subtropical North Pacific Ocean during the last glacial

Kyung E. Lee & Niall C. Slowey

Department of Oceanography, Texas A&M University, College Station, Texas 77843-3146, USA

One of the most controversial results of the CLIMAP[1,2] project's reconstruction of past sea surface temperature (SST) is that large areas of the subtropical Pacific Ocean were warmer during the last glacial period than they are today. This finding has important implications because SST patterns at low to subtropical latitudes strongly influence climate, and SST changes are closely linked with climate fluctuations[3–5]. Until now, a lack of well-preserved, high-resolution marine sediment cores from the region has hindered efforts to confirm these unexpectedly high ice-age SST estimates. Here we use both the oxygen-isotope compositions and species assemblages of planktonic foraminifera in a shallow-water core with high deposition rates near Hawaii to estimate glacial SST of the subtropical North Pacific Ocean. Contrary to the CLIMAP results[2], our data indicate that the annual average SST in this region was ~2 °C cooler during the last glaciation than it is today. These results help to reconcile the marine SST record with inferences drawn from snowline depressions on Hawaii during the last glacial[3,6], and should ultimately yield improved estimates of global climate sensitivity by providing important new constraints on climate model simulations of ice-age cycles.

Located in the central portion of the subtropical North Pacific Ocean, far from confounding influences of oceanic boundary currents and continental landmasses, the Hawaiian Island region is an ideal site at which to investigate the SST 'problem'. Yet attempts to do this using the marine record (including CLIMAP; W. L. Prell, personal communication) have met very limited success. Deep waters in the Pacific are very corrosive to calcium carbonate, so microfossils deposited at most sea-floor sites are poorly preserved and sedimentation rates are low. Dissolution can alter the relative abundance and geochemistry of microfossils while bioturbation of slowly accumulating sediments can mix microfossils of different ages—both processes distort SST records derived from these proxies. At the few sea-floor sites shallow enough to be unaffected by carbonate dissolution, downslope processes confound the records.

Guided by high-resolution seismic imagery, we have identified a shallow-water core that preserves a detailed history of SST variations since the Last Glacial Maximum (LGM). Core PC17 was collected from a moderately sloped portion of the submarine flank of Oahu, Hawaii, located ~6 km off the island's southwestern shore (21.358° N, 158.190° W). SeaMARC II side-scan sonar images indicate that hemipelagic sedimentation occurs at the site of the core and the site is located just down slope from a fossil patch reef which protects it from downslope processes[7]. Annual variability of modern SST there is the same as that in the open ocean[8] and is broadly representative of the region[9]. We cannot demonstrate that this was also the case during the last glaciation, but there is no reason to suspect otherwise given the evidence available at present. The water depth from which the core was recovered (503 m) is well above the calcite lysocline depth[10]. Oxygen-isotope compositions and radiocarbon dates of the mixed-layer-dwelling planktonic foraminifera *Globigerinoides ruber* provide chronological control and indicate that the core's sedimentary record extends from the late Holocene back through the last glacial period (Fig. 1). Sedimentation rates in PC17 during the Holocene (>10 cm kyr^{-1}) and the last glacial period (3–10 cm kyr^{-1}) are higher than those of typical deep sea sediment cores from the central North Pacific. Enhanced sedimentation may result from local topographic focusing. The regular pattern of the δ^{18}O values, the increase in radiocarbon age

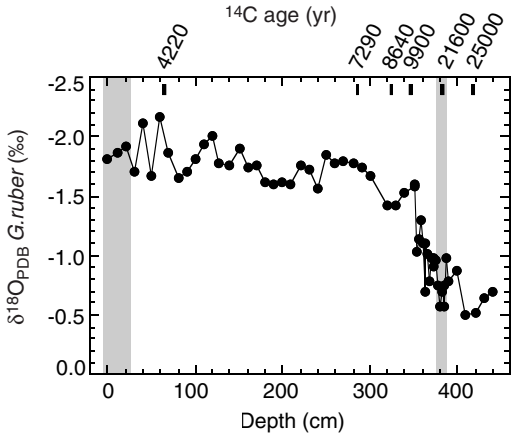

Figure 1 δ^{18}O of *Globigerinoides ruber* in core PC17. The white variety of *G. ruber* (212–250 μm) were analysed following standard methods at Texas A&M University and the Woods Hole Oceanographic Institution. Values relative to the PDB standard are plotted versus depth in the core, and represent the average of two or more analyses. Bars at the top of the plot indicate the depth intervals from which *G. ruber* were taken for radiocarbon dating at the National Ocean Sciences AMS Facility (ages were corrected for surface ocean reservoir age by subtracting 400 yr). Shading indicates data from the recent Holocene and the LGM.